ELSEVIER

EPSL

Was there a wind-driven Tethys circumglobal current in the Late Cretaceous?

N.M.M. Cousin-Rittemard [a,*], H.A. Dijkstra [b], T. Zwagers [b]

[a] *IRMAR, Equipe de Mécanique, Université de Rennes 1, Rennes, France*
[b] *IMAU, Department of Physics and Astronomy, Utrecht University, Utrecht, Netherlands*

Abstract

The problem of the existence of a Tethys circumglobal current (TCC) in the Late Cretaceous continental geometry (Campanian) is addressed. Within an ocean model which is expected to strongly overestimate the wind-driven TCC volume transport, a relatively weak TCC is found for the reconstructed Campanian paleogeography used. As a measure of the strength of the TCC, a circumglobal flow index is introduced. This index is based on volume fluxes through meridional sections within the equatorial part of the domain. The impact of changes in the paleogeography on the TCC is considered by computing steady flows for different shapes of Eurasia. The results on the extent of Eurasia such that a strong TCC appears provide support that no strong wind-driven TCC has existed during the Campanian.
© 2002 Elsevier Science B.V. All rights reserved.

1. Introduction

The ocean circulation is a crucial factor in the present climate because of its role in the meridional transport of heat. It may also have been an important component in the regulation and evolution of past climate states. There are long-standing questions on these past climates, for example on the origin of very warm states during the Me-

sozoic [1,2]. In the Late Cretaceous, global (annual-mean) surface temperatures are estimated to have been about 10°C warmer than today [3]. Although low-latitude temperatures may not have been much higher than those at present, certainly the high-latitude areas were much warmer and consequently earth was approximately ice free [4]. To understand these climate states, a knowledge of the ocean circulation in the geological past is necessary; this has stimulated many modeling studies on the ocean circulation in the Cretaceous [5,6].

An enormous effort over recent decades has resulted in several reconstructions of past bathymetry [7–9]. For the Late Cretaceous, all these reconstructions indicate that a Tethys Ocean existed, which was located between the continental

* Corresponding author. Present address: IRMAR, Equipe de Mécanique, Université de Rennes 1, Campus Beaulieu, 35042 Rennes Cedex, France. Tel.: +33-2-23-23-60-54; Fax: +33-2-23-23-67-90.
  E-mail address: nathalie.rittemard@univ-rennes1.fr (N.M.M. Cousin-Rittemard).

masses in the northern and southern hemispheres. This ocean had two major basins, referred to as the Caribbean Tethys and the Mediterranean Tethys. From biological data, inferences on the direction and strength of the surface currents in the Tethys Ocean can be made [2,10]. For example, Johnson [11] inferred the direction of the surface flow in the Caribbean and the Gulf of Mexico from generic dispersion patterns of rudistic bivalves. These patterns are consistent with a strong southwestward surface current north of the Late Cretaceous South American continent [11]. The faunal distribution in the Late Cretaceous seems to provide evidence [12,13] of the existence of a westward flowing near-equatorial Tethys circumglobal current (TCC).

The TCC is imagined to have had similar characteristics as the present Antarctic circumpolar current (ACC), with relatively large transports through each meridional section [13]. The correspondence between both currents is the absence of zonal boundaries and consequently the absence of a zonal pressure gradient. In this case, a strong zonal flow can be generated by an easterly equatorial wind (TCC) as well as a westerly midlatitude wind (ACC). However, the maxima of the zonal currents are at different latitudes, with different Coriolis parameters, and the impact of these currents on the global circulation may have been quite different [14].

The results from atmospheric–geochemical models (with a simplified mixed-layer ocean as boundary condition) have generated plausible forcing fields of the Cretaceous ocean. In early modeling studies of the mid-Cretaceous ocean circulation [5], a very weak TCC was found. The ocean model used in [5] had a resolution of $5° × 5°$ and four vertical layers. In [15], these results were challenged on the basis that geologic field data suggested a strong westbound surface current along the northern Tethys margin. In the coupled GFDL ocean–atmosphere model for the Maestrichtian, about 17 Sv is found for the Tethys Seaway with a westward core velocity of about 0.11 m/s [16]. The difference between the latter results and the earlier work [5] is attributed not to the different wind structures, but to higher horizontal resolution of the ocean model

$(3.6° × 2.0°$ and 15 vertical levels), which allows representation of less viscous flows [16].

A mid-Cretaceous simulation (about 100 Ma) with four times modern carbon dioxide concentration using the GENESISv2.0 model (described in [17]) has provided wind stress fields and buoyancy fluxes to force the ocean. These were subsequently used in [6] to determine the ocean circulation within the POCM model (described in [18]) using a horizontal resolution of $2° × 2°$ and 20 vertical levels. In the standard setup, there is a weak westward flowing TCC in the mid-Cretaceous circulation [6]. In the Mediterranean Tethys, the circulation is characterized by gyres and only a very narrow Tethys current is simulated hugging the southern margin of the Tethys basin. Sensitivity studies were done of circulation changes versus changes in the shape of the continents. For example, a TCC was only found when the Eurasian continent was 'chopped' below 14°N.

In most of these ocean models, the integration times are fairly short (i.e. 32 years in [16]), which is long enough for equilibration of the wind-driven circulation but not of the thermohaline component of the circulation. A model which only represents the steady-state wind-driven circulation should be quite capable of capturing the essential changes in the strength and directions of the Cretaceous surface currents to changes in continental geometry. Using such a model, we provide an argument against the existence of a strong wind-driven TCC in the Campanian paleogeography (about 80 Ma) as reconstructed in [9]. We introduce a scalar measure of the strength of such a TCC, the circumglobal flow index. Using this index, the critical boundary of the extent of Eurasia such that a TCC is present is calculated. The main result of this paper is that the critical extent of Eurasia to allow a strong TCC is so unrealistic that it is very unlikely that such a current has existed during the Campanian.

2. Model approach

The global ocean domain is defined by all ocean points within a sector $V = [0°, 360°] × [\theta_S,$

θ_N] bounded in meridional direction by $\theta = \theta_S$ and $\theta = \theta_N$. The flow is driven by a wind stress field $\tau(x, y) = \tau_0(\tau^\phi, \tau^\theta)$, where τ_0 is the characteristic amplitude and (τ^ϕ, τ^θ) provide its spatial pattern. The bottom of the ocean is prescribed through a function $z_* = -D + h_{b*}(\phi, \theta)$, where D is the characteristic depth of the ocean; the ocean–atmosphere interface is described by $z_* = h_*$ (the dependent quantities with an * are dimensional) (see Table 1).

In the barotropic case, with water of uniform density ρ_0, the momentum and mass balances can be integrated over the layer depth to give a form of the shallow-water equations. In the usual notation, u_* and v_* are the velocity components of the large-scale flow in eastward and northward directions and $H_* = h_* + D - h_{b*}$ is the thickness of the water column. The dynamical changes of the latter are only due to the changes in the sea surface height. The only dissipative mechanism in the model is the (turbulent) lateral friction. The Reynolds stresses are assumed to depend linearly on the spatial derivatives of the large-scale flow velocity and A_H denotes the horizontal friction coefficient.

Let r_0 and Ω indicate the mean radius and angular velocity of the earth and U be a characteristic horizontal velocity. The governing shallow-

Table 1
Standard values of parameters in the barotropic global shallow-water model

Parameter	Meaning	Value
Dimensional parameters		
r_0	radius of the Earth	6.4×10^6 m
D	equilibrium ocean basin depth	1.0×10^3 m
g	gravitational acceleration	9.8 ms^{-2}
ρ_0	reference ocean density	1.0×10^3 kg m^{-3}
τ_0	wind stress amplitude	1.0×10^{-1} Pa
U	reference horizontal velocity	0.1 ms^{-1}
Ω	Earth's rotation rate	7.5×10^{-5} s^{-1}
Dimensionless parameters		
α	wind stress strength	2.0×10^{-2}
ε	Rossby number	1.0×10^{-4}
F	Froude number	9.8×10^5

Note that the value of the lateral friction parameter A_H (and consequently of the Ekman number E_H) is omitted because it is used as control parameter.
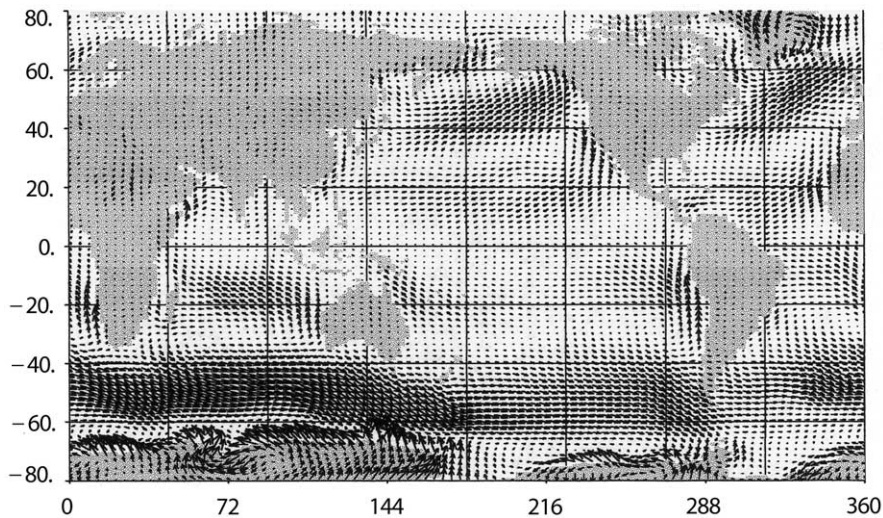
water equations are non-dimensionalized using the characteristic scales r_0, D, U, r_0/U and τ_0 for the length, the layer depth, velocity, time and the wind stress strength, respectively and become

$$\varepsilon\left(\frac{\partial u}{\partial t} + \frac{u}{\cos\theta}\frac{\partial u}{\partial\phi} + v\frac{\partial u}{\partial\theta} - uv\tan\theta\right) - v\sin\theta =$$

$$-\frac{\varepsilon F}{\cos\theta}\frac{\partial h}{\partial\phi} + \alpha\frac{\tau^\phi}{H} + E_H\left(\nabla^2 u - \frac{u}{\cos^2\theta} - \frac{2\sin\theta}{\cos^2\theta}\frac{\partial v}{\partial\phi}\right) \tag{1a}$$

$$\varepsilon\left(\frac{\partial v}{\partial t} + \frac{u}{\cos\theta}\frac{\partial v}{\partial\phi} + v\frac{\partial v}{\partial\theta} + u^2\tan\theta\right) + u\sin\theta =$$

$$-\varepsilon F\frac{\partial h}{\partial\theta} + \alpha\frac{\tau^\theta}{H} + E_H\left(\nabla^2 v - \frac{v}{\cos^2\theta} + \frac{2\sin\theta}{\cos^2\theta}\frac{\partial u}{\partial\phi}\right) \tag{1b}$$

$$\frac{\partial h}{\partial t} + \frac{1}{\cos\theta}\left(\frac{\partial(hu)}{\partial\phi} + \frac{\partial(hv\cos\theta)}{\partial\theta}\right) = 0 \tag{1c}$$

where $H = h - 1 + h_b$ is the total dimensionless layer thickness. To ensure global mass conservation, an integral condition

$$\int_v H\cos\theta\, d\phi d\theta = |\mathcal{V}| \tag{2}$$

is imposed, where $|\mathcal{V}|$ is the dimensionless area of the flow domain. On the lateral boundary Γ of the ocean domain, no-slip conditions are prescribed, i.e.

$$(\phi, \theta) \in \Gamma : u = v = 0 \tag{3}$$

The parameters in Eqs. 1a–1c are the Rossby number ε, the Froude number F, the Ekman number E_H, and the wind stress strength α. Expressions for these parameters are

$$\varepsilon = \frac{U}{2\Omega r_0}; \quad F = \frac{gD}{U^2}; \tag{4a}$$

$$E_H = \frac{A_H}{2\Omega r_0^2}; \quad \alpha = \frac{\tau_0}{2\Omega\rho_0 DU} \tag{4b}$$

Fig. 1. The annual mean value of the wind stress field interpolated from [22] for the present geography of the continents and on a $2° \times 2°$ grid. Only one point in two is plotted for clarity and the wind stress values are scaled by $\max\{|\tau^\phi|, |\tau^\theta|\}$, which is about 0.3 Pa.

Note that, apart from parameters appearing in the pattern of the wind stress forcing, the number of independent parameters for this model is only three. The characteristic velocity U can be chosen as a function of other parameters, reducing the number of parameters in Eqs. 1a–1c by one. When the average depth of the basin and the wind stress amplitude are chosen, the Ekman number E_H is the only (quite uncertain) parameter of the system.

In traditional ocean modeling, the transient flow is computed by solving the initial value problem, starting from a particular initial condition. Here, we solve directly for the steady equations in parameter space, using continuation methods. The steady forms of Eqs. 1a–1c, the integral condition (Eq. 2) and the boundary conditions (Eq. 3) are discretized spatially on the global domain using a second-order finite difference formulation on a staggered $N \times M$ Arakawa C-grid. For example, a $2° \times 2°$ resolution corresponds to $N = 180$ and $M = 90$ on a global domain. After discretization, a system of non-linear algebraic equations results, which is solved by the Newton–Raphson method within a pseudo-arc length continuation method [19].

3. ACC transport

Under the present (Holocene) continental configuration, the ACC in the Southern Hemisphere most resembles a potential TCC. The ACC is a
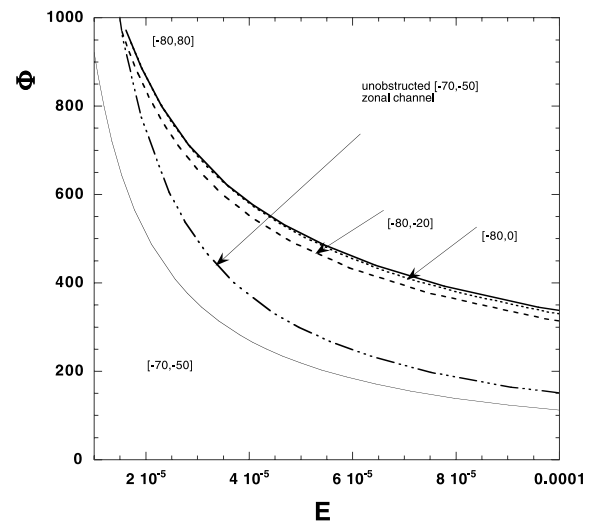

Fig. 2. Plot of different bifurcation diagrams, showing the transport as in (Eq. 5) in Sv versus the Ekman number E_H, for the four different domains considered in Figs. 3 and 4; the curve for the unobstructed channel is also included.
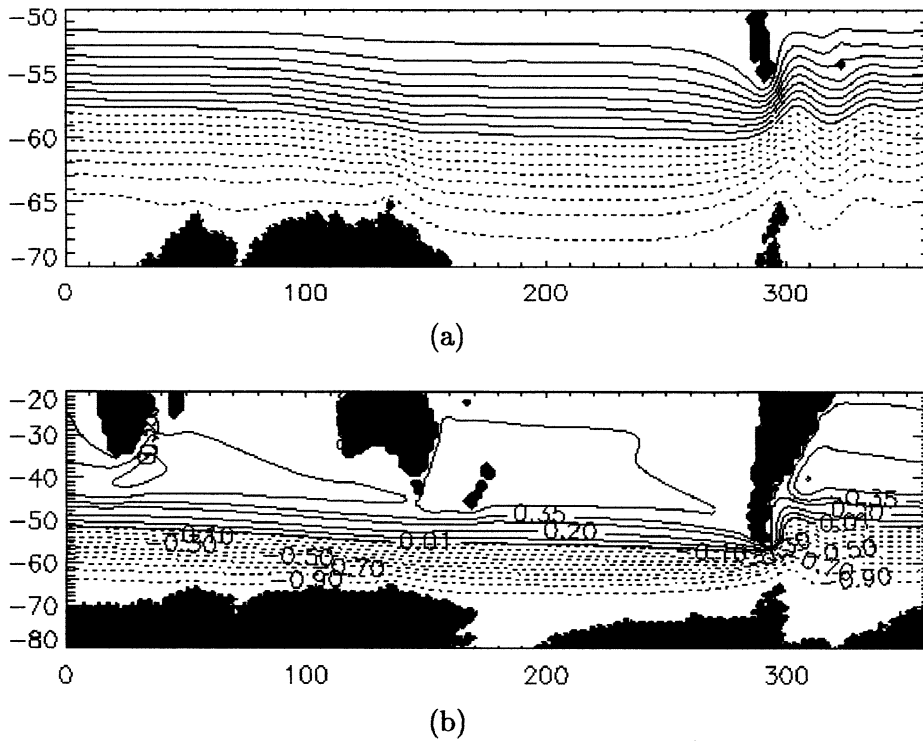
Fig. 3. Contour plots of the solutions for the layer thickness anomaly on different domains. In these plots, the field is scaled by its maximum value. (a) Domain: $[-70, -50]$, $E_H = 10^{-5}$. (b) Domain: $[-80, -20]$, $E_H = 1.51 \times 10^{-5}$.

permanent feature in the Southern Ocean and has a special role in the global ocean circulation by distributing properties between the ocean basins [20]. The flow of the ACC can be characterized by having a time mean volume transport of about 130 Sv. Transport fluctuations have a relative magnitude of 20% and variations have been found on time scales from months up to interannual time scales [21]. The presence of the ACC has a substantial impact on the Atlantic overturning circulation and hence on the meridional heat transport [14].

At first sight, the ACC can be viewed as a zonal flow which is only obstructed by the presence of partial lateral boundaries and bottom topography. With a flat bottom, a zonal channel model of the ACC gives a volume transport which is a factor 10–100 too large for accepted values of the lateral friction coefficient. This transport is also very sensitive to the lateral width of the channel. It is well known that the effect of baroclinic eddies

and the form stresses due to the presence of bottom topography are essential for the magnitude of the Drake Passage transport [21]. The main point of this section is to demonstrate that when the lateral friction is small enough, in the barotropic model of the previous section for a $2° \times 2°$ global continental geometry, the volume transport of the ACC is severely overestimated. The wind stress forcing (Fig. 1) of [22] is used and is interpolated to the grid resolution used. This forcing field represents the westerlies at midlatitudes and trades at low latitudes fairly well and the maximum amplitude of the wind stress is about 0.3 Pa.

In Fig. 2, the maximum eastward transport (in Sv, 1 Sv = 10^6 m^3 s^{-1}) given by

$$\Phi(\phi) = D r_0 U \max_{\theta} \int_{\theta_S}^{\theta} H u \, d\theta \qquad (5)$$

is plotted at the longitude $\phi = 90$ as a function of the Ekman number E_H for five different configu-
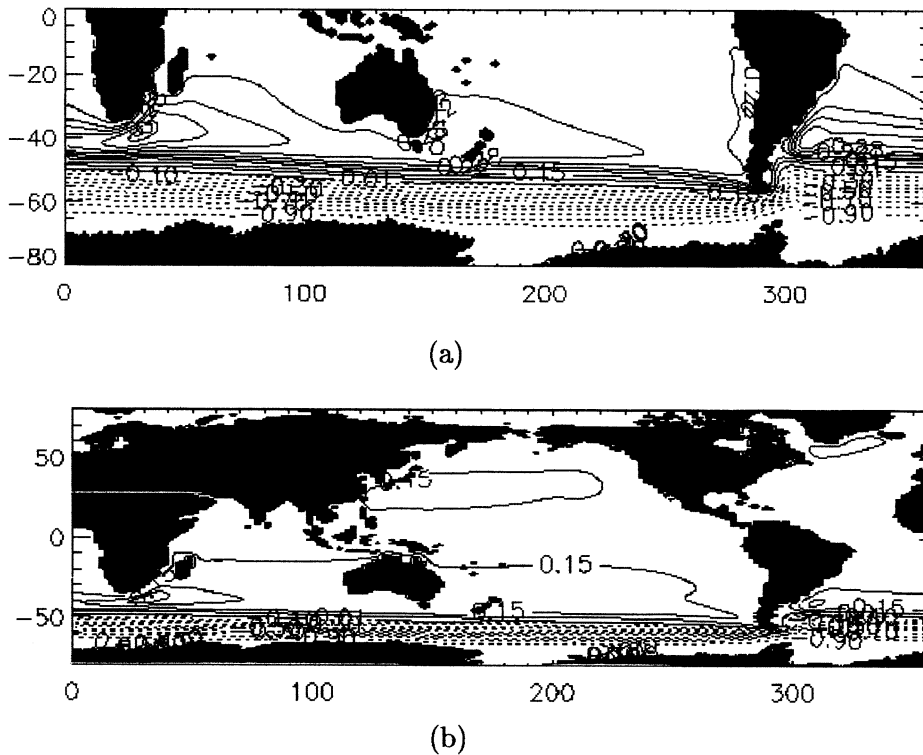
(a)

(b)

Fig. 4. Contour plots of the solutions for the layer thickness anomaly on different domains. In these plots, the field is scaled by its maximum value. (a) Domain: [−80, 0], $E_H = 1.71 \times 10^{-5}$. (b) Domain: [−80, 80], $E_H = 1.62 \times 10^{-5}$.

rations of the domain. The dash-dotted curve is the transport of an unobstructed zonal channel [0, 360]×[−70, −50] for which the transport increases rapidly with decreasing E_H to very unrealistic values (1000 Sv!) at $E_H = 2 \times 10^{-5}$. When continental boundaries are included within the same latitude band, the transport is reduced, but it still is about 500 Sv at $E_H = 2 \times 10^{-5}$. The flow pattern (as a contour plot of the sea surface height) shows the nearly parallel flow before Drake Passage, with a frictionally controlled boundary layer just east of this Passage (Fig. 3a). When the lateral width of the domain is increased to [−80, −20] (dashed curve in Fig. 2), the transport increases. For example, at $E_H = 10^{-4}$, the transport is about 360 Sv compared to 125 Sv for the domain [−70, −50]. The flow pattern in Fig. 3b shows the ACC as a dominant feature in the total flow. In going via the southern hemisphere flow (Fig. 4a) to the global flow (Fig. 4b), the maximum transport of the

ACC increases only slightly (Fig. 2). For all cases, unrealistically large transports are obtained for small values of E_H.

4. TCC transport

In Fig. 5, the continental geometry and annual mean values of the wind stress forcing (reconstructed by GENESISv.2.0) of the Late Cretaceous (Campanian, 80 Ma) [23] period are plotted. The continental configuration and bathymetry as provided respectively by R.M. De-Conto and E.C. Brady (National Center for Atmospheric Research, Boulder, CO, USA) through D. Pollard (Earth System Science Center, Pennsylvania State University, University Park, PA, USA) is obtained from a modern reconstruction for the Campanian based on paleomagnetic information [9]. It can be seen that Australia is still connected to Antarctica; the continental piece
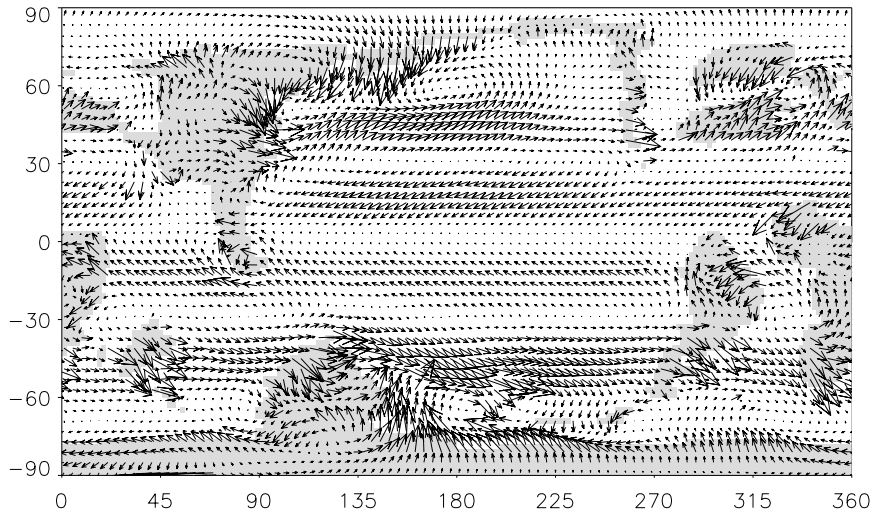
Fig. 5. The global geometry during the Late Cretaceous (Campanian, 80 Ma) on a 2°×2° grid. The reconstructed annual mean value of the wind stress is included as a vector plot; the latter are computed by the GENESIS2.0 model and only one point in two is plotted for clarity. (from: R.M. DeConto, National Center for Atmospheric Research, Boulder, CO, USA).

containing Europe and Asia is referred to as Eurasia.

With respect to the trade winds and the westerlies, these winds have a similar pattern and amplitude as those used in [6]. The steady states of the wind-driven ocean circulation are again calculated on a 2°×2° grid; the average depth D of the ocean is 2717 m and only the flat bottom case is considered. Solutions are computed over the interval $E_H = 10^{-5}$–10^{-4}, to be within the range where the strength of zonal currents is expected to be strongly overestimated.

In Fig. 6a, the steady horizontal velocity is shown for $E_H = 10^{-4}$. There is a strong westward equatorial current in the Pacific which is blocked by the Eurasian continent. The largest part of the incoming flow moves northward in a strong western boundary current, separates from the continent and moves in eastward direction (similar to the present Kuroshio). Note that this current extends to the North American continent and connects to a premature Gulf Stream. The remainder of the flow entering the western boundary layer of the Eurasian continent moves southwards and rounds the tip of Eurasia to form part of the south Indian gyre. The westward current in the Indian Ocean is blocked by the African continent and only a relatively small fraction is able to enter

the Mediterranean Tethys. The major part is deflected southward and takes part in a premature Agulhas Current which hugs the upper boundary of India and connects to the south Pacific gyre system. The southern connection between Pacific and Atlantic is approximately closed but the south Atlantic gyre flow connects to the Pacific through a relatively strong eastward current south of Africa. These major characteristics do not change much at $E_H = 10^{-5}$ (Fig. 6b). However, the effect of the blocking of the Eurasian continent is stronger and the thickness of the western boundary currents has decreased. In both situations, no strong TCC is present although the circumglobal transport seems to be larger in Fig. 6a than in Fig. 6b.

To have a scalar measure of the strength of the TCC current, we define the circumglobal flow index C as:

$$C = \frac{\max_\theta (\int_\theta^{\theta_0} H\, u\, \mathrm{d}\theta)|^{\phi=\phi_{ref}}}{\max_\phi (\max_\phi\, (\int_\theta^{\theta_0} H\, u\, \mathrm{d}\theta)|^\phi} \qquad (6)$$

The integral above calculates at any longitude (ϕ) the transport through a meridional section between two latitudes θ and θ_0. While θ_0 is fixed, θ is determined such that a maximum westward transport appears. We take the reference point in
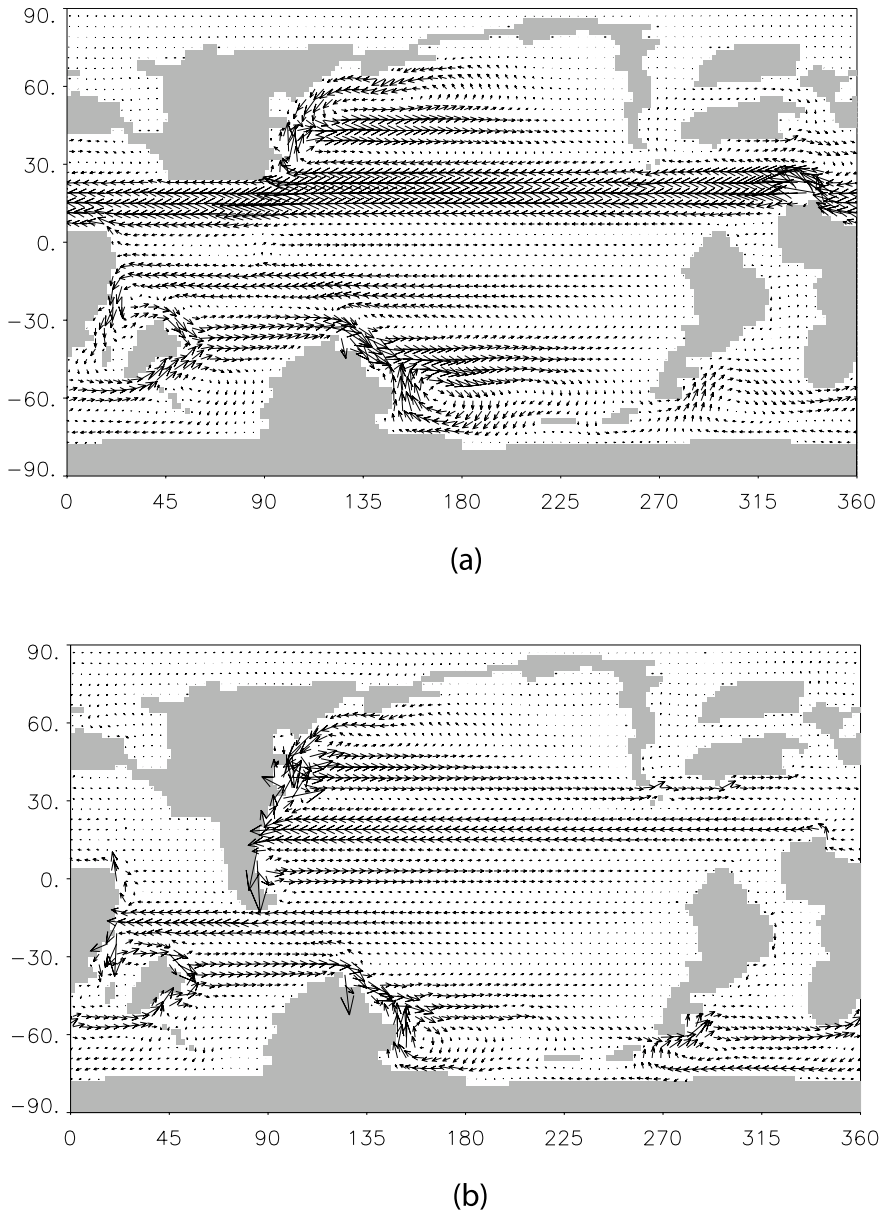
(a)

(b)

Fig. 6. (a) Vector plot of the horizontal velocity field for the steady state at $E_H = 10^{-4}$. The resolution is $2° \times 2°$ and only one point in two is plotted for clarity. Largest vectors indicate velocities of about 0.05 m/s. (b) Same as (a) for $E_H = 10^{-5}$ with largest vectors indicating velocities of about 0.1 m/s. Dimensional horizontal velocities over several sections are plotted in Fig. 8.

the Mediterranean Tethys ($\phi_{ref} = 0°$) and consider the ratio of the maximum transport at this longitude and the maximum westward transport taken over every longitude ϕ of this section. If the maximum transport occurs at the reference point, C will be equal to one. If there is no trans-

port at all at ϕ_{ref}, then C will be zero. If we calculate C, using $\phi_{ref} = 0°$ and with $\theta_0 = 1°$, for the cases in Fig. 6, we find values of $C = 0.23$ for $E_H = 10^{-4}$ and $C = 0.17$ for $E_H = 10^{-5}$, indicating only a weak TCC. Based on the transport values provided in [16], one would 'guess' a

value of C of about 1.0 for the configuration studied.

As in [6], the dependence of the equatorial flow on the southward extent of Eurasia is considered. Note that the positions of the other continental boundaries are unchanged. Changes in the position of the African continent, in particular its northern extent, may also have substantial impact on the westward flows, but this is outside the scope of this paper. Branches of steady states are calculated versus E_H for several shapes of the Eurasian continent which are 'chopped' at some latitude θ_{SA}; for the continental geometry as in Fig. 1, $\theta_{SA} = -9°$. We subsequently consider eight additional cases $\theta_{SA} = -5, -1, 3, 7, 11, 15, 19,$ and $23°$, respectively. For each case, the equilibrium depth of the basin in the area which is 'chopped' is taken as the average depth. The circumglobal flow index C is shown versus θ_{SA} for two values of E_H in Fig. 7. For an Ekman number of 10^{-4}, C increases slightly if the first slices of Eurasia are 'chopped'. If we continue to decrease the extension of Eurasia, this increase becomes larger and C eventually reaches a value of approximately 0.9. The curve for $E_H = 10^{-5}$ shows a much steeper transition at larger θ_{SA} and (except for large θ_{SA}) the value of C is smaller than for $E_H = 10^{-4}$. Due to this sharp transition, one can define a critical point as the maximum slope in the θ_{SA}–C curve; this is the extent θ_{SA} for which a strong TCC appears. The critical point for $E_H = 10^{-4}$ is about $\theta_{SA} = 7°$ and for $E_H = 10^{-5}$ about $\theta_{SA} = 11°$.

For $E_H = 10^{-5}$, meridional sections of the dimensional zonal velocity u_* are plotted at various longitudes (Fig. 8). The different linestyles indicate the different values of θ_{SA} as shown in the caption. At $\phi = 80°$, which is approximately the longitude at which the tail of Eurasia is positioned (Fig. 8a), the westward current strengthens with decreasing extension of Eurasia, consistent with the increase in C. Fig. 8b shows the variation of u_* between $\theta = 15°$ and $\theta = 30°$ for $\phi = 340°$, which is the area above northern Africa. The influence of the extension of Eurasia is strong: as long as $\theta_{SA} < 11°$, zonal velocities remain smaller than approximately -0.04 m/s but if the tail of Eurasia is completely removed, the zonal veloc-
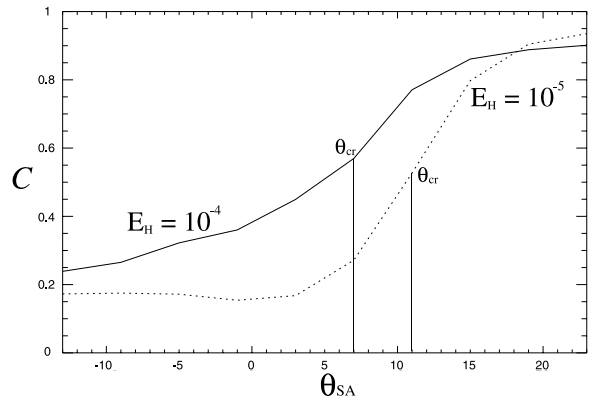

Fig. 7. The circumglobal flow index (C) for various extensions of Eurasia towards the south, represented by θ_{SA}. The solid curve is computed for $E_H = 10^{-4}$ and the dashed curve for $E_H = 10^{-5}$.

ities exceed -0.10 m/s. In Fig. 8c, the change in zonal velocity is shown for the total range of latitudes at $\phi = 180°$. From this, we see that only significant differences occur at Tethyan latitudes. In Fig. 8d,e, changes of the steady flow with θ_{SA} in regions outside the Tethyan region are shown. Although the differences are small, the flow at midlatitudes does respond to changes in the equatorial continental geometry.

To show the difference in the flow patterns computed for different θ_{SA}, horizontal velocity fields were subtracted. The difference field of horizontal velocities between the cases $\theta_{SA} = -1°$ and $\theta_{SA} = -9°$ (Fig. 9a) displays – besides the differences in the Tethyan area – quite some changes in the Antarctic region. The change in the blocking of the westward (near equatorial) flow affects the transport to the South Pacific region and hence the local wind-driven flow in the Antarctic region. A further increase from $\theta_{SA} = -1°$ to $\theta_{SA} = 23°$ (Fig. 9b) does not change much more outside the Tethys region, but the TCC strengthens considerably.

5. Summary and discussion

Global wind-driven ocean circulation patterns for the Late Cretaceous (Campanian) geography have been computed to investigate the conditions
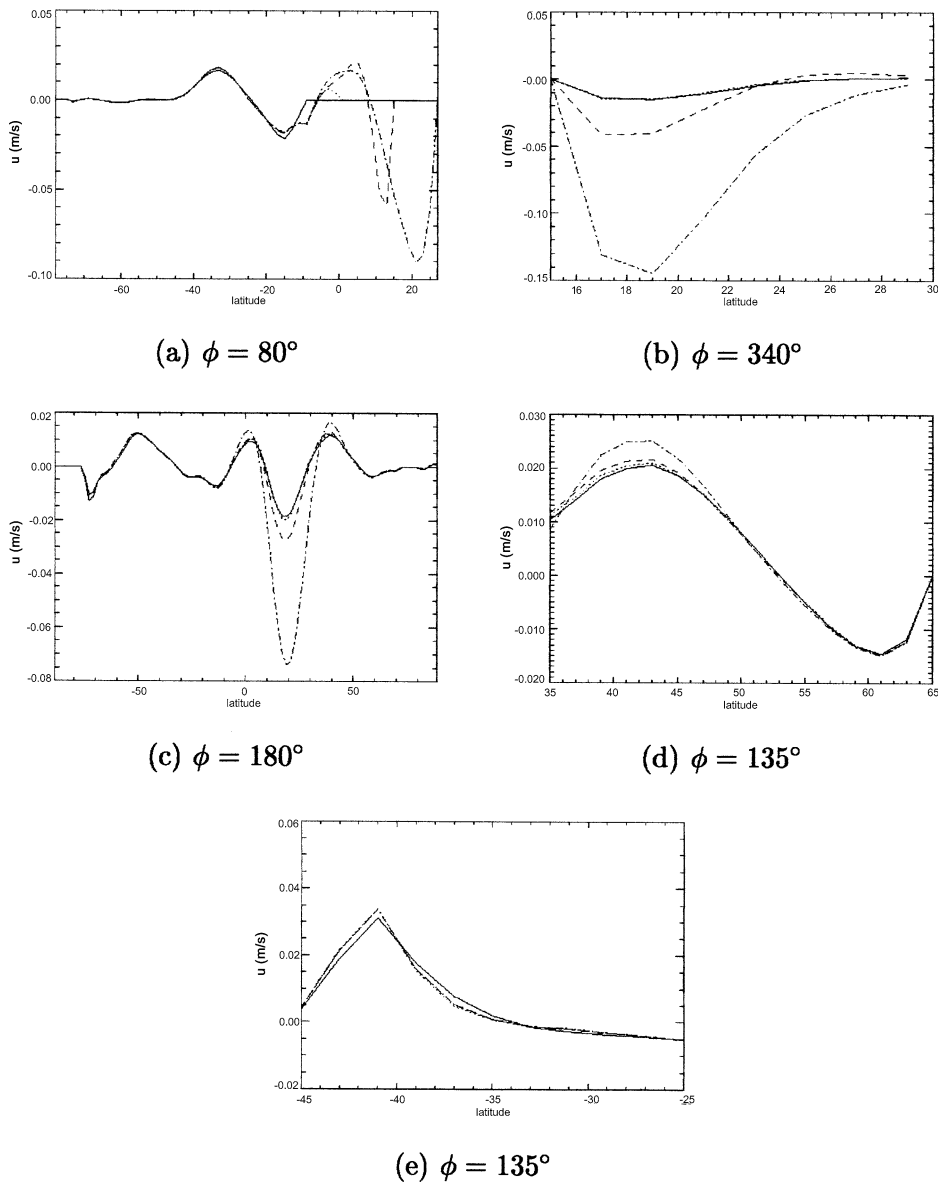
(a) $\phi = 80°$

(b) $\phi = 340°$

(c) $\phi = 180°$

(d) $\phi = 135°$

(e) $\phi = 135°$

Fig. 8. The horizontal dimensional velocity u_* is plotted for $E_H = 10^{-5}$ against a range of latitudes for five different longitudes. The solid curve represents the case with the standard geometry, the dotted curve is for $\theta_{SA} = -1°$, the dashed curve for $\theta_{SA} = 11°$ and the dash-dotted curve is for $\theta_{SA} = 23°$.

of the dynamical existence of a strong TCC and its sensitivity to changes in the extent of the Eurasian continent. Thereto, a circumglobal flow index C was introduced and monitored for different steady-state flow patterns. In the reconstruction of the Campanian used [9], with a model horizontal resolution of $2° \times 2°$, no strong TCC is found and its strength decreases with decreasing values of the lateral friction coefficient (i.e. the Ekman number E_H)

The critical extent of the southern boundary (θ_{SA}) of Eurasia such that a TCC exists, is defined
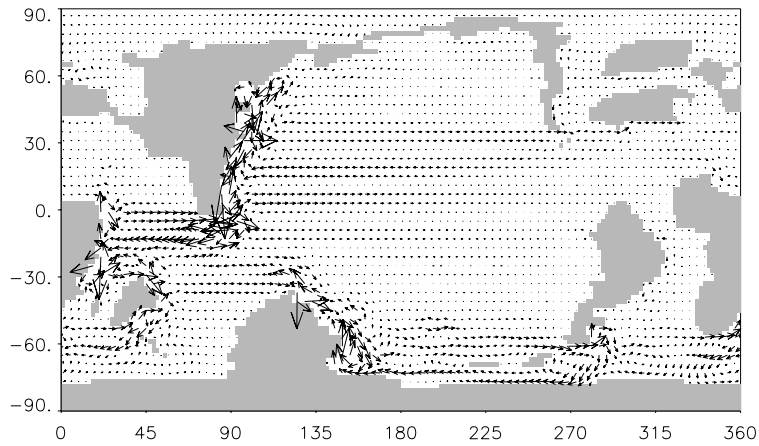
(a)
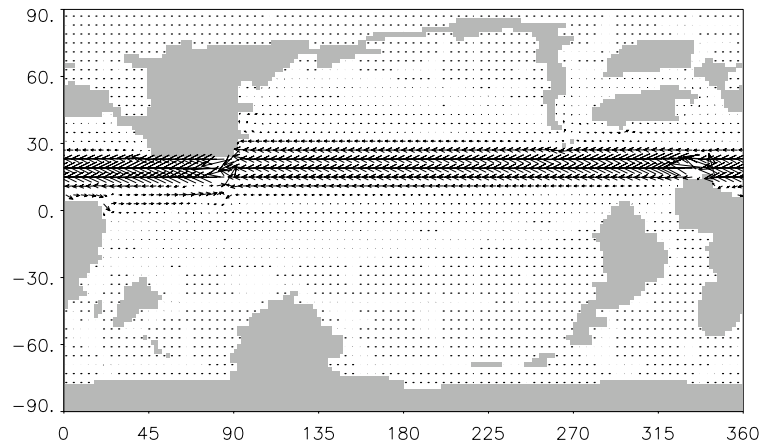
(b)

Fig. 9. Difference between two horizontal velocity fields for different geometries for $E_H = 10^{-5}$. (a) Between $\theta_{SA} = -1°$ and $\theta_{SA} = -9°$. (b) Between $\theta_{SA} = 23°$ and $\theta_{SA} = -1°$.

as the value of θ_{SA} at the maximum slope of the θ_{SA}–C curve. It is located at $\theta_{SA} = 7°$ and $\theta_{SA} = 11°$ for $E_H = 10^{-4}$ and $E_H = 10^{-5}$, respectively. The physics of this difference is not difficult to explain: for a relatively large value of E_H, the boundary layer along the Eurasian continent is rather thick and the flow can pass more easily around the continent. For smaller E_H, the boundary layer thickness decreases and the blocking effect of the continent is much larger. This also explains the much sharper transition in C with θ_{SA} in the small Ekman number case.

Within the model here, in which the surface wind-driven circulation depends on the value of the horizontal friction and the continental geometry, only a qualitative statement can be made on the possibility of a strong TCC in the Campanian geography. From the computation of the transport of the present ACC, we know that such a barotropic model always overestimates the transport if the Ekman number is small enough. With decreasing E_H, the boundary layer near Drake Passage gets thinner and the blocking effect of the continents becomes effectively smaller. For

the Campanian geometry, however, the blocking effect gets larger because there is no region where the zonal pressure gradient vanishes. A decrease in the boundary layer thickness obstructs the flow (due to its high inertia) to round the Eurasian continent. The different latitudes of the mean positions of the two currents (ACC and TCC) in themselves are no factor of importance; when $\theta_{SA} = 23°$, a TCC develops which is similar to the ACC.

Certainly, a barotropic ocean model with a flat bottom is far too simple to describe the complex flow patterns which have been present in the actual Tethys ocean. Both thermohaline processes and the effects of bottom topography likely have been important factors in these flows. However, these factors are not expected to increase substantially the transport of the TCC as modeled here. The combined effects of stratification and bottom topography are known to lead to a strong reduction in the ACC transport [21] compared to the flat-bottomed barotropic case.

A discussion of the different paleogeographies of the Cretaceous can be found in [9]. In all the different continental configurations for the Campanian, the southern end of Eurasia seems to be located south of the equator. It is therefore not very likely that under the wind forcing used here and with the uncertainties in the reconstruction of the Eurasian continent, a mainly wind-driven strong TCC has existed. This does not necessarily contradict the biogeographic data which are available. The flow in the Caribbean Tethys (in the model here) shows substantial westward transport, which is in agreement with the views as in [15] and local reconstructions as in [11]. At this stage, with the available biogeological data it is still too difficult to distinguish an equatorial flow with local westward transport from a 'true' low-latitude circumglobal current.

This leaves the interesting point that in [16] a TCC is present with core velocities of 11 cm/s in the Tethys Seaway. The difference between the continental geometry of the Campanian and Maestrichtian may play a role as well as the different wind field used (there is no land topography in the atmosphere model used in [16]). The occurrence of the TCC in [16] may also be due to

the presence of the thermohaline component of the circulation. Strong negative meridional density gradients in the Tethys Seaway may cause large westward geostrophic zonal velocities through the thermal wind balance. Apart from the fact that this is unclear from the results presented in [16], where no salinity plots are shown, the short integration time (32 years) may also question whether the density field is already equilibrated enough to adequately represent the thermohaline component of the flow. Hence, the issue of the existence of the TCC remains, but the results in this paper have given an argument that it cannot be a mainly wind-driven current.

Acknowledgements

References

[1] T.J. Crowley, G.R. North, Paleoclimatology, Oxford University Press, Oxford, 1991, 349 pp.

[2] C.C. Johnson, E.J. Barron, E.G. Kauffman, M.A. Arthur, P.J. Fawcett, M.K. Yasuda, Middle Cretaceous reef collapse linked to ocean heat transport, Geology 24 (1996) 376–380.

[3] R.M. DeConto, E.C. Brady, J. Bergengren, W.W. Hay, Late Cretaceous climate vegetation, and ocean interactions, in: B.T. Huber, K.G. MacLeod, S.L. Wing (Eds.),

Warm Climates in Earth History, Cambridge University Press, Cambridge, 2000, pp. 275–296.

[4] T.J. Crowley, J.C. Zachos, Comparison of zonal temperature profiles for past warm time periods, in: B.T. Huber, K.G. MacLeod, S.L. Wing (Eds.), Warm Climates in Earth History, Cambridge University Press, Cambridge, 2000, pp. 50–76.

[5] E.J. Barron, W.H. Peterson, Model simulation of the Cretaceous ocean circulation, Science 244 (1989) 684–686.

[6] C.J. Poulsen, D. Seidov, E.J. Barron, W.H. Peterson, The impact of paleogeographic evolution on the surface oceanic simulation and the marine environment within the mid-Cretaceous Tethys, Paleoceanography 13 (1998) 546–559.

[7] E.J. Barron, Cretaceous plate tectonic reconstructions, Palaeogeogr. Palaeoclimatol. Palaeoecol. 59 (1987) 3–29.

[8] C.R. Scotese, J. Golonka, Paleographic Atlas, PALEO-MAP Project, University of Texas at Arlington, TX, 1992.

[9] W.W. Hay, R.M. DeConto, C.N. Wold, K.M. Wilson, S. Voigt, M. Schultz, A. Wold-Rossby, W.C. Dullo, A.B. Ronov, A.N. Balukhovsky, E. Söding (Eds.), Evolution of the Cretaceous Ocean-Climate system, Geological Society of America, Spec. Pap. 332 (1999) 1–48.

[10] S. Voigt, W.W. Hay, R. Höfling, R.M. DeConto, Biogeographic distribution of late Early to Late Cretaceous rudist-reefs in the Mediterranean as climate indicators, in: E. Barrera, C.C. Johnson (Eds.), Evolution of the Cretaceous Ocean-Climate System, Geological Society of America, Spec. Pap. 332 (1999) 91–104.

[11] C.C. Johnson, Evolution of Cretaceous surface current circulation patterns, Caribbean and Gulf of Mexico, in: E. Barrera, C.C. Johnson (Eds.), Evolution of the Cretaceous Ocean-Climate System, Geologial Society of America, Spec. Pap. 332 (1999) 329–344.

[12] W.A. Gordon, Marine life and ocean surface currents in the Cretaceous, J. Geol. 81 (1973) 269–284.

[13] C.R. Lloyd, The mid-Cretaceous Earth: paleogeography, ocean circulation and temperature, J. Geol. 90 (1982) 393–413.

[14] H. Bjornsson, J.R. Toggweiler, The climatic influence of Drake Passage, in: D. Seidov, B.J. Haupt, M. Maslin (Eds.), The Oceans and Rapid Climate Change, Geophys. Monogr. 126, Am. Geophys. Union, Washington, DC, 2001, pp. 243–260.

[15] K.B. Follmi, M. Delamette, Model simulation of mid-Cretaceous ocean circulation, Science 251 (1991) 94.

[16] A.B.G. Brush, Numerical simulation of Cretaceous Tethys circumglobal current, Science 275 (1997) 807–810.

[17] S.L. Thompson, D. Pollard, Greenland and Antarctic mass balances for present and doubled atmospheric CO_2 climates from the GENESIS Version-2 Global Climate Model, J. Clim. 10 (1997) 158–187.

[18] D.R. Stammer, R. Tokmakian, A. Semtner, C. Wunsch, How well does a 1/4° global circulation model simulate large scale oceanic observations?, J. Geophys. Res. 101 (1996) 25779–25811.

[19] H.B. Keller, Numerical solution of bifurcation and nonlinear eigenvalue problems, in: P.H. Rabinowitz (Ed.), Applications of Bifurcation Theory, Academic Press, New York, 1997, pp. 359–384.

[20] W.J. Schmitz, On the interbasin-scale thermohaline circulation, Rev. Geophys. 33 (1995) 151–173.

[21] S.R. Rintoul, C. Hughes, D. Olbers, The Antarctic Circumpolar Current System, in: J.C.G. Siedler, J. Gould (Eds.), Ocean Circulation and Climate, Academic Press, New York, 2001, pp. 271–302.

[22] K.E. Trenberth, J.G. Olson, W.G. Large, A global ocean wind stress climatology based on ECMWF analyses, Technical report, National Center for Atmospheric Research, Boulder, CO, 1989.

[23] E.C. Brady, R.M. DeConto, S.L. Thompson, Deep water formation and poleward heat transport in the warm climate extreme of the Cretaceous (80 Ma), Geophys. Res. Lett. 25 (1998) 4205–4208.